Assessing glacier thickness changes with multi-temporal UAV-derived DEMs: The evolution of Forni Glacier over the period 2014–2022

International Journal of Applied Earth Observation and Geoinformation 140 (2025) 104547

Contents lists available at ScienceDirect

International Journal of Applied Earth Observation and Geoinformation

journal homepage: www.elsevier.com/locate/jag

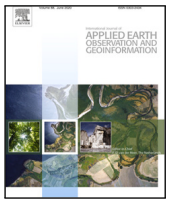

Assessing glacier thickness changes with multi-temporal UAV-derived DEMs: The evolution of Forni Glacier over the period 2014–2022

Valeria Belloni [a], Davide Fugazza [b,*], Kevin Hanson [c], Marco Scaioni [d], Martina Di Rita [e]

[a] Department of Civil, Building and Environmental Engineering, Sapienza University of Rome, Via Eudossiana 18, Rome, 00184, Italy
[b] Department of Environmental Science and Policy, University of Milan, Via Giovanni Celoria 10, Milan, 20133, Italy
[c] Leica Geosystems AG, Heinrich Wild Strasse 201, Heerbrugg, 9435, Switzerland
[d] Department of Architecture, Built Environment and Construction Engineering, Politecnico di Milano, Via Ponzio 31, Milan, 20133, Italy
[e] Interuniversity Department of Regional and Urban Studies and Planning, Politecnico di Torino, Viale Mattioli 39, Turin, 10125, Italy

ARTICLE INFO

Keywords:
UAV photogrammetry
Multi-temporal UAV data
DEM generation
DEM co-registration
Climate change
Glacier monitoring

ABSTRACT

Glaciers in the European Alps are undergoing significant retreat and thickness decrease due to climate change, contributing to sea-level rise and impacting the mountain environment and its biodiversity, tourism and local economy. Unmanned Aerial Vehicle (UAV) photogrammetry offers cost-effective methods for high-resolution glacier monitoring. However, multi-temporal UAV-based data usually must be improved in terms of consistency due to possible variable survey conditions, requiring precise co-registration. This study presents a novel application of the Iterative Closest Point algorithm of the NASA Ames Stereo Pipeline to co-register Digital Elevation Models (DEMs) from UAV images of Forni Glacier (Italy) collected under different conditions from 2014 to 2022. We co-registered the DEMs generated from Structure-from-Motion/Multi-View Stereo matching within a pairwise structure. This process demonstrated clear improvements in data consistency, with mean and median values tending to zero, RMSEs below 0.50 m, and NMADs below 0.32 m. The comparison of co-registered DEM highlighted glacier thickness losses at the terminus reaching 50 m, with side areas showing smaller reductions of around 25 m between 2014 and 2022.

1. Introduction

As in other areas of the Earth, glaciers in the Alps are experiencing the effects of climate change, impacting the economy and various ecosystems. Glacier retreat affects, among others, water supply for hydroelectric energy production, revenues from the tourism industry, local environment and biodiversity, and contributes to sea-level rise. While the contribution of glacier meltwater to energy production in the Alpine region is often less than 10% (D'Agata et al., 2018; Schaefli et al., 2019), it reaches more than 20% during the summer months when demand is at its peak (D'Agata et al., 2018). High glacier losses increase meltwater availability, initially beneficial for hydroelectric energy production, but lead to long-term shortages with serious consequences for the energy industry (Milner et al., 2017). In terms of tourism, glacier retreat, downwasting, as well as phenomena such as glacier darkening (Di Mauro and Fugazza, 2022) and macro- and microplastic contamination (Crosta et al., 2022), lead to significant changes in the glacial and periglacial landscape (Diolaiuti and Smiraglia, 2010), altering the tourist perception of glacier geosites (Salim, 2023). Summer and winter ski activities on glaciers are also severely affected by the ongoing retreat. Also, since glaciers are often on the route to popular mountain peaks, the increase in the frequency of collapses at the glacier terminus can introduce a source of hazards for hikers and mountaineers (Fugazza et al., 2018). Finally, while glaciers have long been considered lifeless environments, they have recently been found to harbour large communities of bacteria (Franzetti et al., 2017) and small invertebrates (Gobbi and Lencioni, 2021); thus, glacier retreat threatens the survival of cold-adapted species and could eventually lead to a loss of biodiversity.

Evaluating these impacts requires accurate and detailed knowledge of glacier variations over time. Photogrammetry from UAV (Unmanned Aerial Vehicle) images has emerged as an effective and low-cost tool to investigate these variations. Indeed, the generation of Digital Elevation Models (DEMs) and orthophoto mosaics at very high resolution enables detailed glacier geomorphological mapping (Azzoni et al., 2017; Belloni et al., 2023) and accurate investigation of glacier dynamics and thickness changes (Immerzeel et al., 2014; Karimi et al., 2021; Van Tricht et al., 2021; Lamsters et al., 2022; Ioli et al., 2022; Di Rita et al., 2020). Most of the works related to this topic have focused on

* Corresponding author.
E-mail address: davide.fugazza@unimi.it (D. Fugazza).

https://doi.org/10.1016/j.jag.2025.104547
Received 6 February 2025; Received in revised form 25 March 2025; Accepted 16 April 2025
Available online 12 May 2025

evaluating the detailed dynamics of glaciers on short temporal scales, from a seasonal (Benoit et al., 2019; Rossini et al., 2018; Kraaijenbrink et al., 2016; Bash et al., 2018; Immerzeel et al., 2014) to a two- or three-year time span (Fey and Krainer, 2020; Karimi et al., 2021; Lamsters et al., 2022; Di Rita et al., 2020; Van Tricht et al., 2021). Bearzot et al. (2022) investigated the kinematics of Gran Sometta Rock Glacier using UAV surveys from 2016 and 2019. Ioli et al. (2022) presented the results achieved using UAV data collected on Belvedere Glacier over a longer time span, between 2015 and 2020. Vivero and Lambiel (2024) presented the results in the elevation changes of rock glaciers between 2016 and 2021. Finally, some authors have presented results of studies covering longer periods, which however integrate DEMs obtained from UAV images with DEMs from airborne or satellite imagery (e.g. De Gaetani et al., 2021; Eskandari et al., 2024).

Investigating a long series of data collected with UAVs at multiple epochs usually presents challenges. First, targets used as Ground Control Points (GCPs) to give the collected data a ground constraint and enable it to be in the same reference frame may be difficult to establish in challenging environments such as glaciers. This can result in suboptimal target distribution or the absence of GCPs. In these cases, the generated DEM should be co-registered with a second georeferenced DEM to establish a common reference frame and evaluate the glacier change (Di Rita et al., 2020). UAVs equipped with RTK-GNSS (Real-Time Kinematics - Global Navigation Satellite System) partially reduce the problem related to the absence of GCPs. However, these types of UAVs have become popular only in recent years (Belloni et al., 2022; Dall'Asta et al., 2017) while older data could not be likely collected in RTK mode. Also, RTK can easily be lost or unavailable on glaciers. Secondly, the different UAVs used during surveys, the meteorological conditions and the flight plan influence the quality of each photogrammetric block and the generated DEMs in terms of visible details (derived from the Ground Sample Distance - GSD), accuracy of the reconstruction, and geolocation (Di Rita et al., 2020). For all these reasons, when investigating glacier evolution over a long period, co-registration of multi-temporal DEMs is necessary to minimize the errors due to inaccurate geolocation that can otherwise affect the evaluation of the glacier morphological change. This is even more important when integrating multi-platform data, which usually also present uneven photo scales between epochs.

Different approaches enable removing offsets between multi-temporal overlapping DEMs. Two categories of DEM co-registration methods exist: shift-based solutions and approaches based on 3D rigid transformation estimations (Li et al., 2023). The first ones usually compute the shift between two DEMs by minimizing the sum of their vertical distances. However, they do not estimate the effect related to rotation and scaling and they have been widely tested for co-registering DEMs generated from satellite data where translations represent the major effect. Following this approach, Berthier et al. (2007) calculated the mean shift between DEMs by minimizing the standard deviation of the difference between the two DEMs outside the glaciers using a 2D linear regression. Nuth and Kääb (2011) presented a simple and robust co-registration method for DEM pairs using the elevation difference residuals and the elevation derivatives of slope and aspect to provide a 3D shift vector between two DEMs. The second category of methods estimates a 3D conformal transformation (i.e., translations, rotations and scaling between two DEMs) and is suitable for DEMs with complex misalignments, including horizontal and rotational discrepancies. This category includes 3D surface matching techniques such as feature point-based methods (Aguilar et al., 2012), methods based on centroids of subwatersheds (Li et al., 2017), feature line-based methods (Karkee et al., 2008), multi-feature based surface matching method (Wu et al., 2013), the Iterative Closest Point (ICP) algorithm (Besl and McKay, 1992) and its successive developments (Pomerleau et al., 2013), and the least squares 3D surface matching algorithm (Gruen and Akca, 2005; Akca, 2010). Among these, the ICP algorithm has been widely adopted for point clouds and DEM co-registration. Specifically for DEMs, the NASA Ames Stereo Pipeline (ASP) implements the ICP algorithm (Pomerleau et al., 2013) to determine the rigid-body transformation (nine rotation and three translation terms) and co-register DEMs. The software has been widely investigated for co-registering DEMs generated from satellite data and altimetry data, as well as global DEMs (Shean et al., 2016, 2019, 2020). Recent works have investigated the possibility of joining multi-epoch images in a single block in the photogrammetric processing based on the Structure-from-Motion (SfM)/ Multi-View Stereo (MSV) matching pipeline (Westoby et al., 2012; Micheletti et al., 2015; James and Robson, 2012) solving the problem of co-registration between epochs (Feurer and Vinatier, 2018; Andaru et al., 2022; Genzano et al., 2024). However, this approach highly depends on the quality, resolution, and radiometric content of images and is usually challenging in high mountain environments where even stable areas may be affected by erosion processes, accumulation of transported material, and snow (Genzano et al., 2024).

In this paper, after presenting the data collected with high-resolution UAV surveys over the area of Forni Glacier in the 2014–2022 time span, we investigate the potential of ICP for co-registering DEMs generated under non-uniform conditions (i.e., variable numbers of GCPs and different types of UAVs, GNSS connection services, and photogrammetric processing software) using the ASP software. Finally, we evaluate the evolution of Forni Glacier in the 2014–2022 period. To our best knowledge, this paper presents the longest series of data collected over a glacial area with UAV surveys, and the first application of the ASP software to UAV DEM co-registration.

2. Study area and data

Forni Glacier is one of the largest valley glaciers in the Italian Alps, located in the protected Stelvio National Park (Ortles-Cevedale group, Lombardy Alps) and with an area of 10.50 km^2 in 2016 (Paul et al., 2020). The glacier is an important geosite (Senese et al., 2023), and its meltwater feeds one of the main hydroelectric power plants (245 MW) in Valtellina Valley. Forni Glacier recession has been continuous since the 1980s: in 2015, the easternmost of the three ice streams forming the glacier tongue became separated from its accumulation basin, while the western tongue has been largely covered by debris in recent times (Belloni et al., 2023). Other evident signs of the glacier morphological changes are the rapid retreat of the terminus, with frequent occurrence of collapsing areas (Fugazza et al., 2018) and the formation of neo supraglacial moraines as a result of differential ablation (Azzoni et al., 2017).

The UAV surveys of this study focus on the glacier tongue, including the eastern and central parts. While the extents differ between the UAV surveys, all of them cover the position of the glacier terminus at the time of each flight, parts of the proglacial area in front of the terminus and areas at the sides of the terminus which can be considered stable. Fig. 1 shows the location of Forni Glacier, together with the glacier outlines in 2016 (Paul et al., 2020) and the extent of the areas covered by the UAV surveys for the period of interest.

The UAVs used in the different surveys changed over the years, due to technological improvements and changing regulations in the field of drones, leading to various data acquisition strategies. While some surveys have been described in previous research (Fugazza et al., 2018; Scaioni et al., 2019; Belloni et al., 2023, 2022), here we overview all their characteristics.

2.1. 2014 dataset

On 28th August 2014, a survey was conducted with a fixed-wing Swinglet CAM developed by Sensefly. The drone carried a Canon IXUS 127 HS 16 Mpx compact digital camera (4.3 mm focal length) and was flown in autopilot mode with an average flying height of approximately 380 m above ground. Flights were carried out with a forward and side overlap of 70% and 60%, resulting in a coverage of 2.21 km^2. The

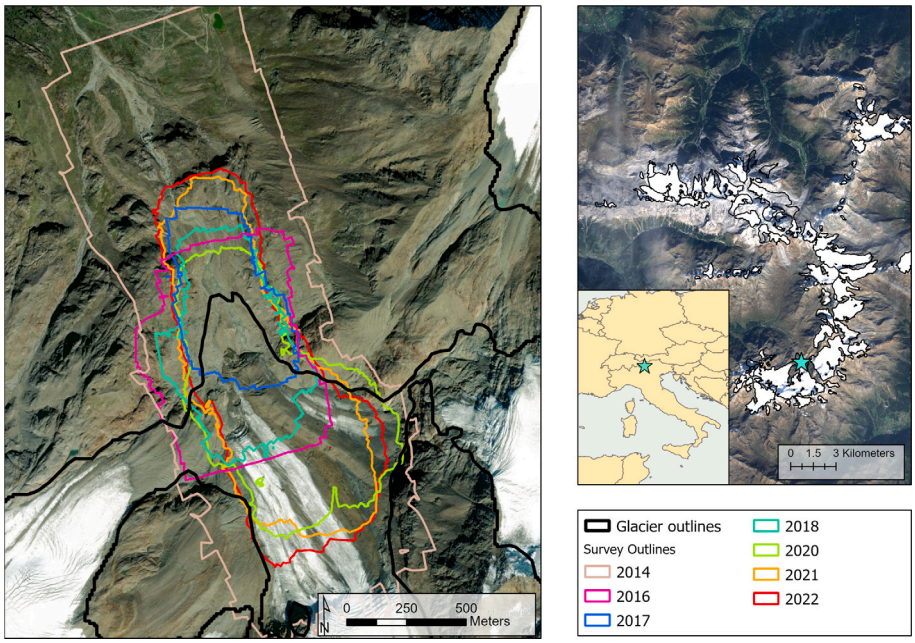

Fig. 1. Location of Forni Glacier and outlines of the UAV surveys. The glacier outlines updated to 2016 are from Paul et al. (2020). The background image in the left panel is from Bing maps®. The right image is from a Sentinel-2 scene acquired on 29/9/2016.

camera was operated in automatic shooting mode, selecting the best combination of shutter speed, ISO and aperture (Fugazza et al., 2018). In total, 86 RGB images were acquired. No GCPs were placed for this photogrammetric block, resulting in the availability of only the onboard GNSS navigation-grade data for georeferencing.

2.2. 2016 dataset

Two surveys were conducted on 30th August and 1st September 2016. The UAV employed in this survey was a customized quadcopter incorporating a Tarot frame 650 size, VR Brain 5.2 Autopilot & APM Arducopter 3.2.1 Firmware, with a GPS+Glonass antenna and carrying a Canon Powershot ELPH 320 16 Mpx digital camera with 4.3 mm focal length (Scaioni et al., 2017). The UAV was operated from two take-off and landing sites on the sides of the glacier, to gain elevation and maintain line-of-sight operations, with a flying height of 50 m above the elevation of the take-off sites and an average of 180 m above ground. 288 RGB images were acquired in manual shooting mode (Scaioni et al., 2019), with shutter speed set to 1/2000 s to reduce motion blur, aperture at F/2.7 and ISO sensitivity at 200. The UAV was flown in autopilot mode with a 70% forward and side overlap, covering an area of 0.59 km^2 (Fugazza et al., 2018). Before the surveys, 8 GCPs consisting of targets made of white textile material with a red dot in the centre (Scaioni et al., 2017) were spread on- and off-glacier (3 and 5, respectively), mostly covering the terminal and lateral parts. Their position was measured using a Leica Geosystems 1200 GNSS receiver communicating in RTK mode with a reference station set up close to Branca Hut (2505 m a.s.l). All targets were used as GCPs for image processing and DEM generation.

2.3. 2017 dataset

To reconstruct a collapse that occurred at the glacier terminus during the summer, a survey was conducted on 15th October 2017. For this survey, we used the same UAV employed in 2016 with the same camera setup, flying from the right hydrographic flank of the glacier to gain elevation for take-off and maintain a relative flying height of approximately 135 m above ground. This survey covered the smallest area among those presented in this study (0.29 km^2). 161 RGB images were acquired (Scaioni et al., 2019) during four flights, with the camera set in manual mode. The clear sky with no clouds allowed setting a low ISO sensitivity of 100 while retaining bright images. The shutter speed was set to 1/1600 s and the aperture to F/2.7. Five plastic targets with an alternating red-green pattern were placed on the ground before the survey (2 on- and 3 off-glacier) to be used as GCPs. Their position was measured using a Leica ATX1230 GNSS receiver in fast static mode with respect to a master GNSS station located close to the Branca Hut.

2.4. 2018 dataset

A survey was conducted on 20th August 2018, using the same UAV, camera and setup of 2016 and 2017. Six flights were carried out from the hydrographic left side of the glacier to maintain a flying height of approximately 20 m relative to the elevation of the take-off site and 90 m above ground. 299 RGB images were acquired with the camera set in manual mode. The shutter speed was set to 1/2000 s, the lowest possible setting, while the other parameters were allowed to vary. Aperture ranged between F/2.7 and F/8 and ISO sensitivity between 100 and 400. While such low ISO values resulted in a few dark images, this was done to reduce noise and did not prevent image matching. Eight plastic targets as in 2017 were placed on the ground before the survey (5 on- and 3 off-glacier at the terminus and downvalley). All of them were used as GCPs and their position was measured as in 2017. The area covered by this survey was 0.40 km^2.

2.5. 2020 dataset

Three surveys were carried out on 20th, 21st, and 22nd August 2020. The UAV employed during this mission was a DJI Phantom 4 RTK. The drone carried an FC6310R camera with a 20 Mpx sensor and a focal length of 8.8 mm. The UAV stores satellite observation data for Post Processing Kinematic (PPK) when the RTK connection is lost or unavailable. In the campaign, the DJI Phantom 4 RTK was combined with a D-RTK 2 high-precision GNSS mobile station to allow UAV RTK navigation. Also, a local GNSS base station (a Leica GS18 T GNSS receiver) was established close to the Branca hut to store raw GNSS data and compute an accurate position of the base itself using permanent stations. This enabled the computation of PPK positions of UAV tracks

Table 1
Summary of UAV survey characteristics.

Year	UAV	Camera	Flight height	Forward and side overlap	GSD	Area
–	–	–	(m)	(%)	(cm/px)	(km^2)
2014	Swinglet CAM	Canon IXUS 127 HS	380	70–60	10.9	2.21
2016	Customized quadcopter	Canon Powershot ELPH 320	180	70–70	5.3	0.59
2017	Customized quadcopter	Canon Powershot ELPH 320	135	70–70	4.1	0.29
2018	Customized quadcopter	Canon Powershot ELPH 320	90	70–70	2.8	0.40
2020	DJI Phantom 4 RTK	DJI FC6310R	100	80–75	2.2	0.65
2021	DJI Phantom 4 RTK	DJI FC6310R	100	80–75	2.8	0.71
2022	DJI Phantom 4 RTK	DJI FC6310R	100	80–75	2.5	0.80

necessary to integrate the RTK measurements of the targets over the glacier given the lack of GSM cell coverage (Belloni et al., 2023). The UAV was flown with a flying height of approximately 100 m above ground, with 80% and 75% forward and side overlap. The camera was operated in automatic shooting mode, selecting the best combination of shutter speed, ISO and aperture (Belloni et al., 2022). In total, 1172 RGB images were acquired and 20 plastic and natural targets were used as GCPs for this survey, both on- and off-glacier. The plastic targets were made of white and black textile material, while the natural targets were made of stones and wood (Belloni et al., 2022). The area covered by this survey was 0.65 km^2.

2.6. 2021 dataset

Three surveys were carried out on 19th, 20th, and 21st August 2021 using the same devices and configuration adopted during the 2020 survey (Belloni et al., 2022). The same camera settings were used in this case. In total, 1131 RGB images were acquired and targets (either artificial or natural) were placed on- and off-glacier for this survey. Thirteen targets were used as GCPs and 11 as independent Check Points (CPs). The area covered by this survey was 0.71 km^2.

2.7. 2022 dataset

Three surveys were carried out on 18th, 19th, and 20th August 2022 with the same configuration and UAV adopted during the 2020 and 2021 campaigns. The same camera settings were used in this case as well. In total, 2101 RGB images were acquired and 23 targets were placed for this survey on- and off-glacier (15 as GCPs and 8 as CPs). The area covered by this survey was 0.80 km^2. Data collection and processing of this dataset are described in Belloni et al. (2023).

In Table 1 and Fig. 2 we present the main characteristics and the distribution of GCPs and CPs for each survey.

3. Methodology

The workflow is divided into: photogrammetric DEM generation, DEM co-registration and DEM differencing (Fig. 3).

3.1. Photogrammetric DEM generation

We processed the datasets from the 2014, 2016, 2017, and 2018 missions using Leica Infinity and Agisoft Metashape photogrammetric software packages. We used Leica Infinity to post-process the GNSS data of the collected target positions in 2016, 2017 and 2018 using a reference base close to Branca Hut (in 2016) or from the SPIN GNSS regional network (in 2017 and 2018). Agisoft Metashape (ver. 2.1.1) was adopted for SfM, including target marking, image orientation, camera self-calibration, MVS matching for Dense Point Cloud (DPC) generation, and DEM interpolation. We used the software "high accuracy" settings for image orientation and MVS. For the former stage, this option involved using original RGB images without downsampling. For the latter stage, a factor 2 downsampling was adopted (Agisoft, 2024). We choose this latter setting as a trade-off between the quality of the expected final products and the processing time. When possible, we evaluated the precision of the results using the collected targets as GCPs. For the datasets from 2020, 2021 and 2022 we processed the data using only Leica Infinity taking advantage of the last available versions of the software (starting from ver. 3.4) and the new tool for UAV GNSS track post-processing in PPK mode. Leica Infinity combines the PPK strategy for UAV tracks and the SfM technique integrated with bundle block adjustment, to achieve the best possible result in terms of accuracy. The aim was also to compensate for different sources of errors common in mountain areas. Firstly, we post-processed the raw GNSS data from the receiver located close to the Branca Hut using raw GNSS data acquired by a network of permanent stations (ETRF2000 reference system) as reference. Then, we used this receiver as a master station to post-process the UAV GNSS tracks collected during each UAV flight (Belloni et al., 2023). Finally, we performed the standard photogrammetric pipeline implemented in the software: target marking, image orientation, DPC generation, and DEM interpolation. We performed auto-calibration and estimated camera intrinsics based on the available GCPs. We evaluated the precision and accuracy of the processing using the acquired targets as GCPs and CPs. For the 2020 datasets, due to signal loss at the Branca master station and suboptimal target distribution, we could not post-process a few UAV tracks. Therefore, we used all the targets as GCPs to improve the processing and evaluated the image block precision only, due to the lack of independent CPs. The 2020 and 2021 methodology for DPC and DEM generation was partially described in Belloni et al. (2022), in which we focused on the potential of UAV GNSS track post-processing over a smaller area. In the present work, we extended the area of interest to generate a larger DEM of 2020 and 2021 for glacier thickness change computation. Finally, the 2022 DEM generation and validation are described in detail in Belloni et al. (2023). We generated all the DEMs with a ground spatial resolution of 20 cm and we exported them in the Universal Transverse Mercator (UTM) coordinate system, zone 32N (EPSG: 32632), orthometric height to facilitate DEM co-registration and glacier elevation change computation.

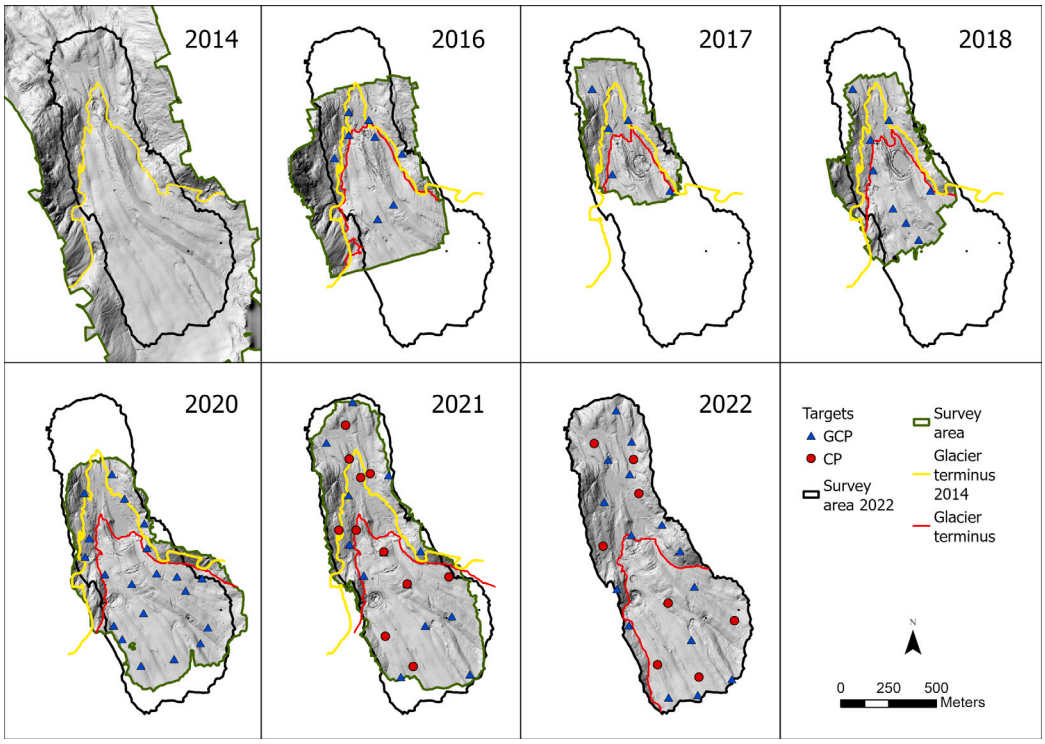

Fig. 2. Distribution of Ground Control Points (GCPs) and Check Points (CPs) for each survey. The area of each survey and the area of the 2022 survey, the glacier terminus in the specific year and the terminus in 2014 are also shown as a reference.

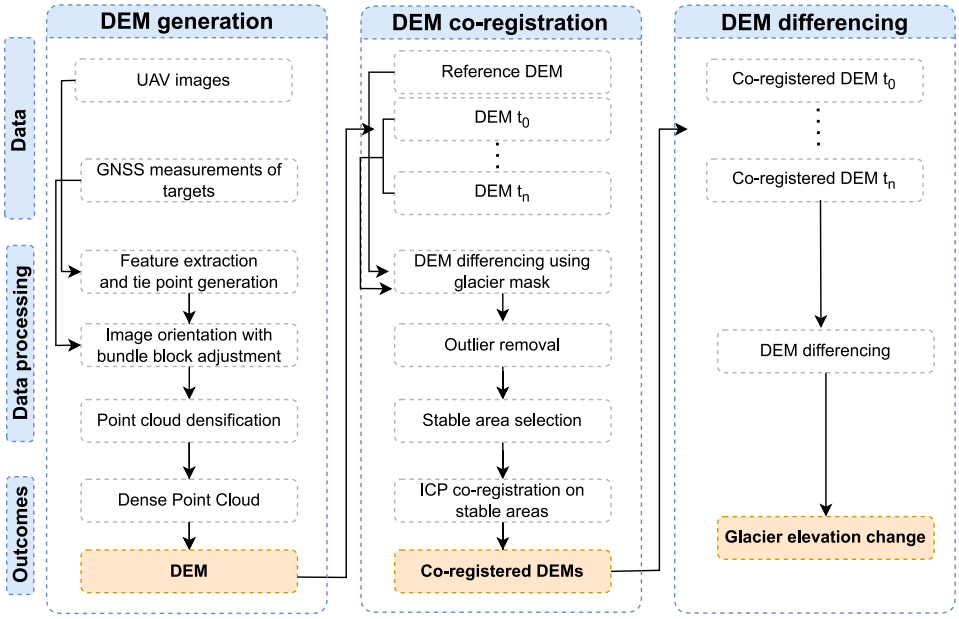

Fig. 3. Proposed workflow.

Table 2
DEM precision and accuracy.

	2014	2016	2017	2018	2020	2021	2022
GCPs		8	5	8	20	13	15
CPs						11	8
Precision (m)		0.29	0.06	0.10	0.07	0.04	0.04
Accuracy (m)						0.04	0.06

3.2. DEM co-registration

To compute the glacier elevation changes more accurately, we co-registered all the generated DEMs. We used the 2022 DEM of Forni Glacier as a reference since it covers a wide area and is the most accurate available DEM over the glacier. We co-registered all the other input source DEMs to it, considering only the stable areas outside the glacier that we assume did not change between the image acquisitions. We clipped the reference and the other input DEM to a common intersection and masked the glacier surface using the 2014

Table 3
Co-registration accuracy of the pairwise structure.

		Mean (m)	Median (m)	Std Dev (m)	RMSE (m)	NMAD (m)	Stable areas (km^2)
2022–2014	before	1.32	1.32	0.47	1.41	0.47	0.21
	after	**−0.03**	**−0.01**	**0.24**	**0.25**	**0.15**	
2022–2016	before	−0.63	−0.56	0.63	0.89	0.65	0.11
	after	**−0.11**	**−0.04**	**0.48**	**0.49**	**0.32**	
2022–2017	before	0.66	0.78	0.72	0.98	0.90	0.14
	after	**0.02**	**0.01**	**0.33**	**0.34**	**0.20**	
2022–2018	before	0.35	0.31	0.42	0.54	0.44	0.10
	after	**0.14**	**0.04**	**0.35**	**0.38**	**0.23**	
2022–2020	before	−0.02	−0.02	0.06	0.06	0.05	0.07
	after	**0.00**	**0.00**	**0.06**	**0.06**	**0.05**	
2022–2021	before	−0.07	−0.08	0.07	0.10	0.05	0.16
	after	**0.00**	**0.00**	**0.07**	**0.07**	**0.04**	

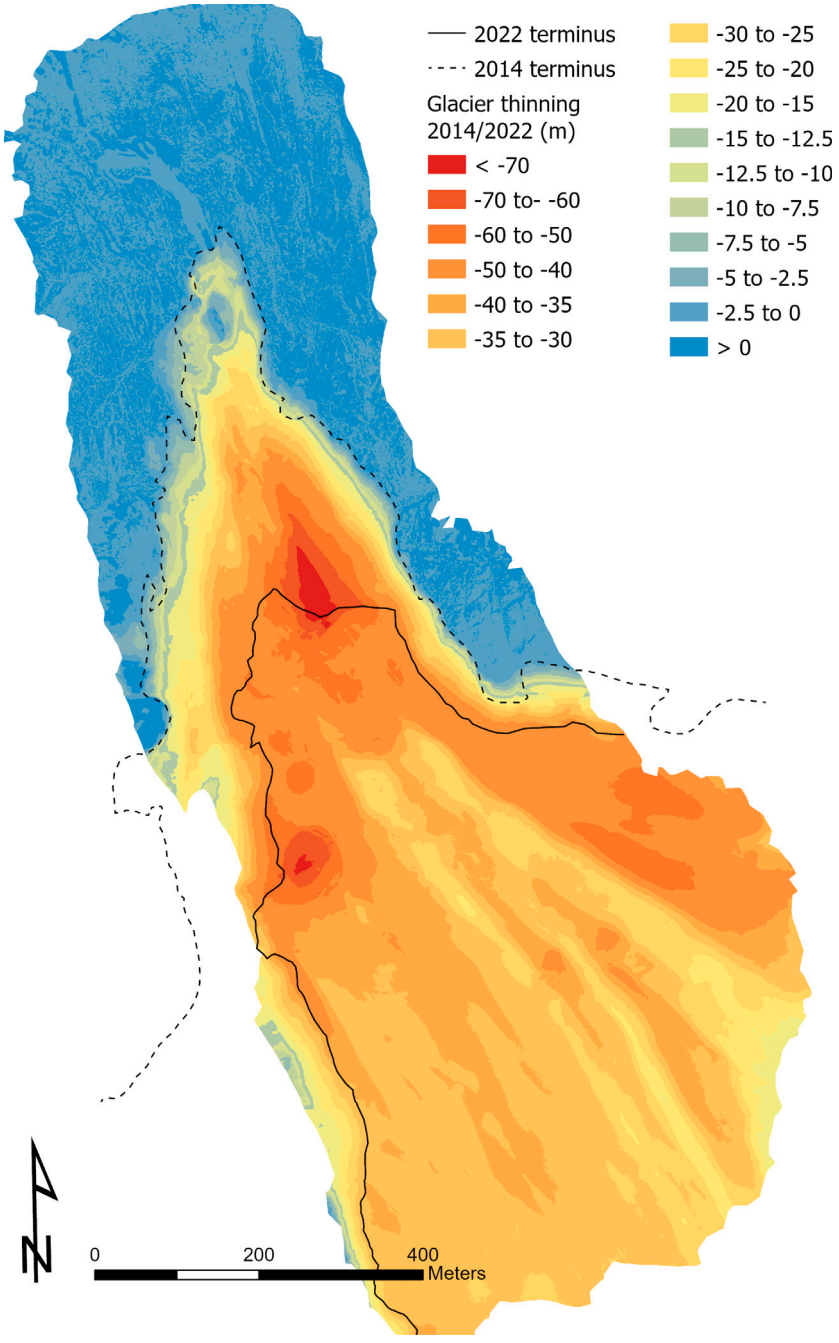

Fig. 4. Glacier thinning between 2014 and 2022.

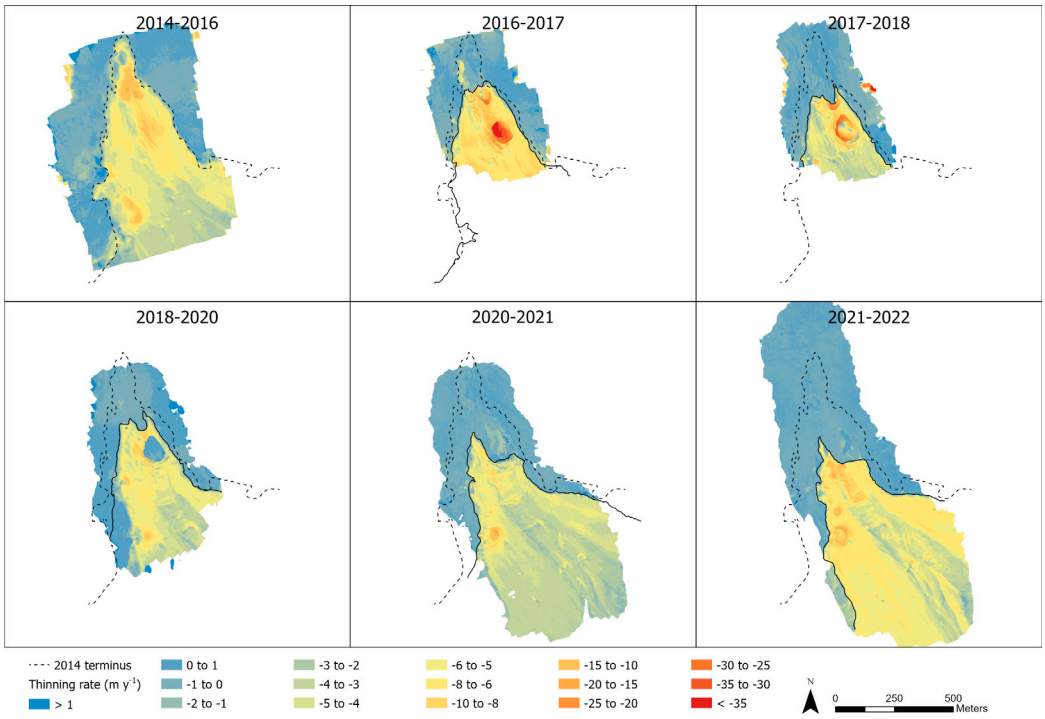

Fig. 5. Glacier thinning rate between each consecutive DEM pair from 2014 to 2022. The black solid line indicates the glacier outline for the first year in each comparison.

outline. We computed the DEM difference and removed the outliers by setting a threshold based on the median and the Normalized Median Absolute Deviation (NMAD) (median ± 2NMAD). We repeated this procedure to identify the common stable areas separately for each DEM pair to maximize the areas for co-registration. Then, we used the ICP co-registration workflow implemented in the open-source NASA ASP (Beyer et al., 2018) through the ASP pc_align utility to automatically co-register each input source DEM to the 2022 reference DEM (ASP, 2025). The pipeline allows using a point-to-plane or point-to-point ICP algorithm (Pomerleau et al., 2013), that iteratively improves the transformation required to minimize offsets. The software output is a 3D transformation (3 translations and 3 rotations). We used the default point-to-plane algorithm since it works better for control data with adequate spatial distribution over surfaces with sufficiently variable slope and aspect (Shean et al., 2016). We computed the transformation using a two-step procedure to avoid a correlation between the estimated rotations and translations. Firstly, we limited the transformation to a 3-parameter translation without estimating rotations and applied the inverse of the ICP solution to the input DEM. Then, we computed translation and rotation terms and we applied the estimated transformation. In the second step, the translations were approximately zero and, in this way, we could independently compute rotations. To evaluate the quality of the co-registration procedure, we computed the difference between the reference 2022 DEM and all the other DEMs for each pixel over the stable areas before and after co-registration. Then, we calculated five standard statistical metrics of the differences to evaluate the co-registration accuracy: mean, median, standard deviation (Std Dev), Root Mean Square Error (RMSE) and NMAD.

3.3. DEM differencing

After co-registration, we compared multi-temporal DEMs by differencing each consecutive DEM pair over their common area, including both stable and glacial areas. In this way, we generated maps of the glacier elevation change rate for each consecutive DEM pair and the total loss by differencing the 2014 and 2022 DEMs. Finally, we defined longitudinal and transverse sections that cross some of the glacier's interesting features, including the medial moraine and collapsing areas.

4. Results

4.1. DEM generation

We produced the 2014 DEM without GCPs, relying entirely on the UAV GNSS navigation but we could not evaluate precision and accuracy due to the lack of available targets. For the 2016, 2017 and 2018 datasets, we used the few available targets (5–8) as GCPs and computed only the geolocation precision. We obtained a precision in terms of RMSE of $\Delta 3D$ of the GCPs equal to 0.29 m, 0.06 m, and 0.10 m for every epoch, respectively. We generated the 2020 DEM using all the available targets as GCPs, due to the loss of RTK signal between the UAV and its base station and the difficulties of post-processing a few UAV tracks due to battery failure of the Branca master station. Therefore, we used the available targets to evaluate only the precision of image block geolocation (RMSE of $\Delta 3D$ of the GCPs) equal to 0.07 m. Finally, for 2021 and 2022 we adopted the targets as both GCPs and CPs and evaluated the geolocation precision and accuracy of the image block. The 2021 DEM validation highlighted an overall mean precision and accuracy (RMSE of $\Delta 3D$ of GCPs and CPs, respectively) of 0.04 m. For the 2022 DEM, the overall mean precision and accuracy are 0.04 m and 0.06 m, respectively.

A summary of the geolocation precision and accuracy of all the generated DEMs before co-registration is shown in Table 2.

4.2. DEM co-registration

Table 3 shows the statistical metrics of each DEM pair differencing before and after co-registration.

For each pair, it is worth noticing a clear improvement in all the statistics with mean and median values close to zero after co-registration, which highlights a bias removal for all the DEM pairs, and RMSEs below 0.50 m which provides information on the accuracy of the co-registration. The most evident improvement after co-registration refers to the 2014 DEM generated without GCPs, relying entirely on the UAV GNSS navigation. The 2014 DEM presents the worst geolocation accuracy before co-registration with mean and median values of

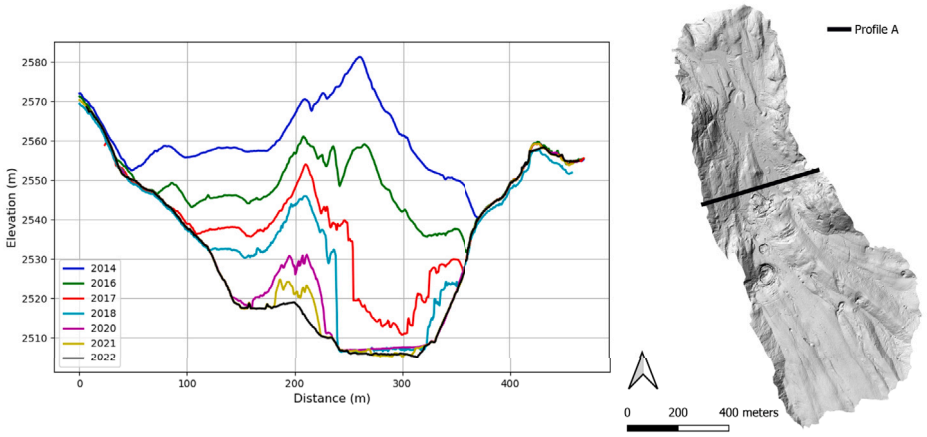

(a) Section A.

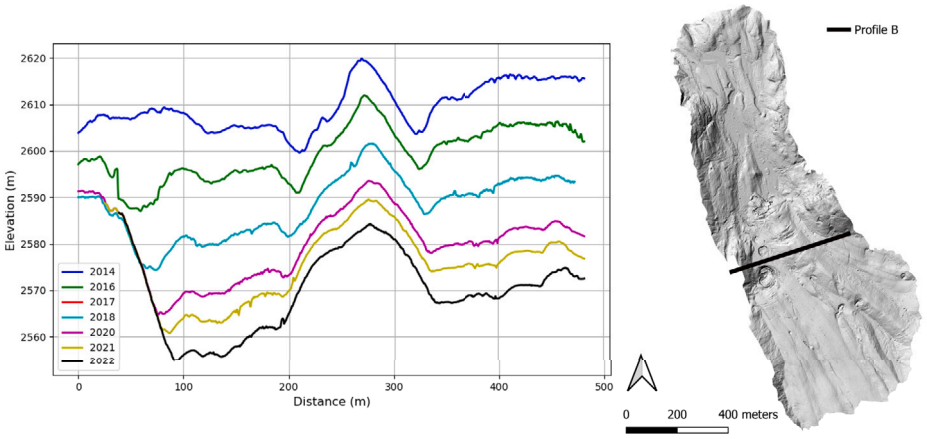

(b) Section B.

Fig. 6. Transverse sections. Section B is not covered by the 2017 survey.

1.32 m, RMSE of 1.41 m and NMAD of 0.47 m. For the 2016, 2017, and 2018 DEMs, the statistics before co-registration highlight the maximum mean and median values of 0.78 m, RMSEs of 0.98 m, and NMADs of 0.90 m. In 2020 and 2021 statistics before co-registration highlight better results with mean and median values of a few centimetres, RMSEs below 0.10 m and NMAD of 0.05 m. The improvement after co-registration is minimal and results highlight mainly a bias removal of a few centimetres, as these DEMs were generated with a higher number of targets, RTK UAVs and UAV track post-processing.

4.3. Glacier thickness changes

The analysis of the UAV-derived DEMs acquired between 2014 and 2022 reveals a significant reduction in glacier thickness over the study period. As shown in Fig. 4, the most pronounced changes occurred in the ablation zone near the terminus, driven primarily by increased ice melt caused by prolonged exposure to high temperatures. Elevation losses at the terminus reached approximately 50 m, with side areas showing comparatively smaller reductions of around 25 m, likely due to the rapid melting of exposed ice during the first part of the data series. In addition, localized collapsing areas experienced ice thinning of more than 70 m. In contrast, the areas that experienced lower than average thinning are those covered by the glacier medial moraine, where the ice loss was less than 30 m over 8 years. During the same period, the glacier terminus retreated by more than 450 m, highlighting the impressive extent of glacial changes.

Fig. 5 illustrates the annual glacier thinning rates and terminus retreat progression based on consecutive DEM pairs. The results indicate an average elevation loss of 4–6 m year^{-1}, with pronounced thinning near the glacier front and areas of local collapse largely exceeding these values. For instance, 2016–2017 saw a dramatic elevation loss exceeding 35 m near the terminus due to a collapse that persisted until 2020 when the ice in the affected area completely melted, as can be seen in the comparison between 2018 and 2020. In the DEM difference 2020–2021, the collapse was no longer visible, reflecting the retreat of the terminus and the complete loss of ice in that area. The comparison between 2020 and 2021, and 2021 and 2022 also reveals the emergence of a second collapsing area on the western side of the glacier, with losses of around 20 m year^{-1}. The areas outside the glaciers' outline occasionally show thinning rates not equal to zero due to the changing morphology of these areas in terms of moving rocks and sediment reworking by the water flowing out of the glacier.

For a local comparison, we selected three sections inside the area of interest (A, B and C) to analyse longitudinal and transverse profiles that cross areas of interest over the glacier, including the medial moraine and collapsing areas at the terminus. In addition, for Section A we included stable areas at the borders of the glacier. Figs. 6(a) and 6(b) show the two transverse Sections A and B, while Fig. 7(a) presents the longitudinal Section C. Fig. 6(a) highlights the evident changes in glacier elevation with larger differences in the central area of the glacier and a local collapse area evident since 2017 until complete ice melt-out, with an ice loss larger than 40 m between 2016 and 2017.

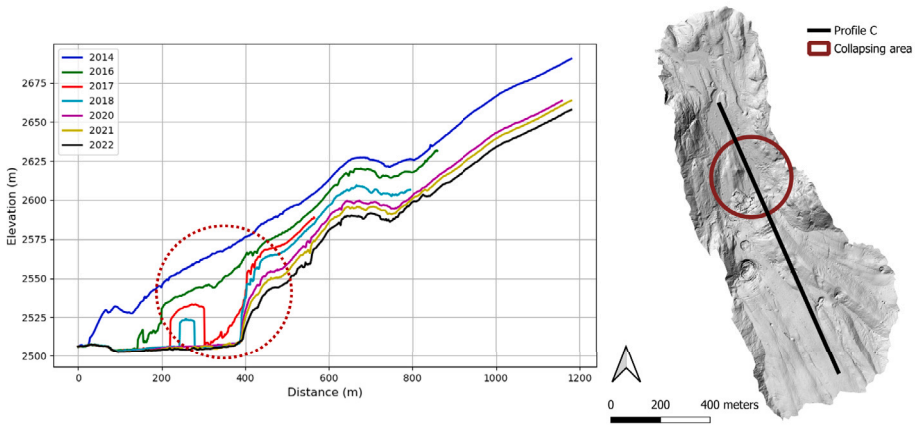

(a) Section C.

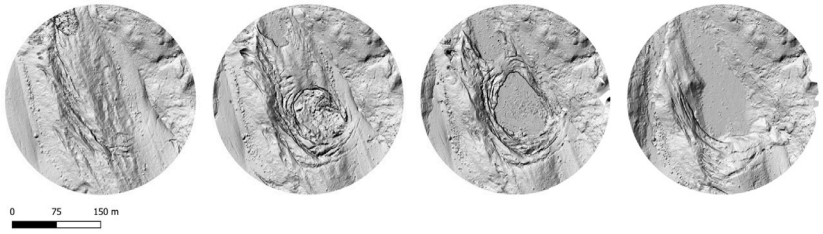

(b) The evolution of a local collapsing area at the terminus. From left to right 2016, 2017, 2018 and 2020 DEMs.

Fig. 7. Longitudinal section.

Fig. 6(b) highlights the evident elevation change of the entire profile with reduced losses corresponding to the medial moraine, where changes average 3–6 m year^{-1} compared to up to 10–20 m year^{-1} over the rest of the profile. Finally, Fig. 7(a) shows a significant height loss at the glacier terminus until 2018 and gradually decreasing at higher elevations. The local collapsing area at the terminus is shown in progression in Fig. 7(b). The maximum height loss here is reached between 2016 and 2017, with just short of 39 m.

5. Discussion

In the Alps, recent glacier changes have been documented with UAVs at several sites, on multi-annual and seasonal time scales, alone and in combination with other aerial surveys. Monitored sites include Vadret da Morteratsch (Rossini et al., 2018; Van Tricht et al., 2021), Gorner Glacier (Benoit et al., 2019), Vernagtferner (Geissler et al., 2021), Belvedere Glacier (Ioli et al., 2022), Brenva Glacier (Fugazza and Troilo, 2024), Miage (Westoby et al., 2020) and Popera glacier (Securo et al., 2024). Similar studies have also been carried out in the Himalayas (Brun et al., 2018; Vincent et al., 2016), Kunlun mountains (Che et al., 2020), Tibetan Plateau (Fu et al., 2022) and Svalbard (Lamsters et al., 2022). While the areas monitored in the different studies vary, considering the ablation area, the changes of Forni Glacier lie in the upper range of what is generally observed at glacier sites in terms of averages and maximum changes of ice losses. On Forni Glacier, we observed an average glacier thinning of 34.21 ± 11.67 m between 2014 and 2022, or 4.28 ± 1.46 m year^{-1}. Rossini et al. (2018) observed 4.1 m of ice losses at Vadret da Morteratsch during the ablation season 2016; a similar thinning rate is reported by Westoby et al. (2020) at Miage glacier between 2015 and 2018, while lower values are observed by Fu et al. (2022) at Dagongba glacier on the Tibetan Plateau in the ablation season 2018 (2.81 m), by Brun et al. (2018) on Changri Nup glacier in the Himalayas between 2011 and 2015 (0.93 m year^{-1}) and by Securo et al. (2024) on Popera glacier in the Dolomites between 2021 and 2022 (2.46 m). Even higher rates of ice thinning compared to Forni Glacier are reported by Che et al. (2020) for Baishui River glacier in the Kunlun mountains in the ablation season 2018 (6.58 m) and by Fugazza and Troilo (2024) for Brenva Glacier in the Mont Blanc region of the Alps (13.22 m between 2019 and 2020). We further evaluated the ice thinning of Forni Glacier from 2014 to 2022 with respect to the main topographic parameters (elevation, aspect and slope, see Fig. 8). In this period, glacier thinning increased up until 2580–2590 m a.s.l., when it reached −42.19 m, and then stabilized in the higher portions of the glacier tongue (−30.25 m at 2700 m a.s.l.). As regards the aspect, similar thinning is observed in all sectors, with a peak of −35.17 m for SW. It has to be noted that the glacier slopes predominantly face NE or SW. The influence of slope is more evident, as glacier thinning is highest on gentle slopes (−36.75 m at 0°) and lowest with highly sloping surfaces (−13.87 at 90°), most likely as a result of the lower solar radiation on north facing sloping surfaces. Figs. 4 and 8 also show the effect of morphological factors, e.g. the glacier collapses which are mostly located in elevation bands between 2550 and 2650 m a.s.l. These features are typical of downwasting glaciers and an increasingly common sight in the Alps, as shown by Egli et al. (2021) for glaciers in Switzerland and more tragically in the case of Marmolada glacier (Bondesan and Francese, 2023).

6. Conclusions

This study provides the most extensive dataset derived from photogrammetric processing from UAV missions of the Forni Glacier in the Italian Alps, which span nearly a decade (2014–2022). It represents a novel application of NASA ASP for co-registering multi-temporal DEMs obtained from UAV data and analysing glacial dynamics with high-resolution datasets. The co-registration workflow proved to be instrumental in enhancing the consistency and relative accuracy of

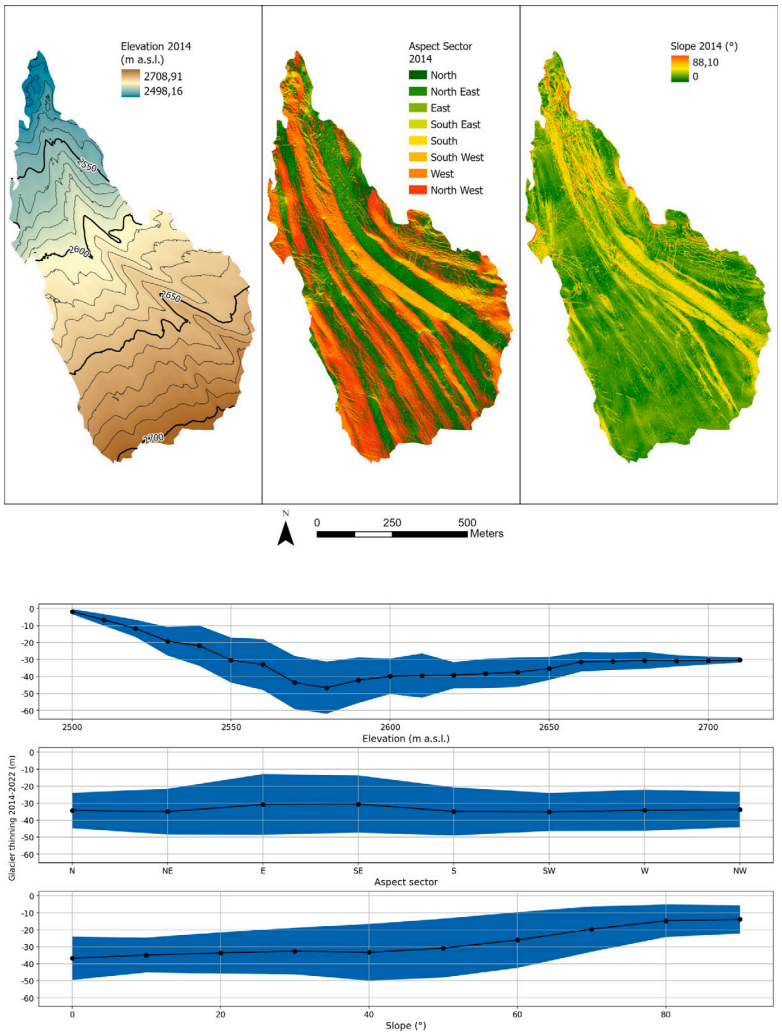

Fig. 8. Glacier thinning from 2014 and 2022 with respect to the main topographic parameters (elevation, aspect and slope). Top: elevation, aspect and slope of Forni Glacier in 2014 in the common area of the 2014 and 2022 surveys. Bottom: glacier thinning as a function of elevation (10 m elevation bands), aspect sector and slope (10° slope bands). The black dots indicate the average in each elevation/slope band or aspect sector, while the blue area is one standard deviation.

the DEMs under varying survey conditions. Quantitatively, the co-registration process significantly reduced biases and minimized errors, achieving RMSE values below 0.50 m and NMAD below 0.32 m. These improvements underscore the robustness and reliability of this approach for multi-temporal glaciological studies. In addition, analysis of co-registered DEM revealed pronounced changes in the Forni Glacier, with an average glacier thinning of 34.21 ± 11.67 m and a glacier terminus retreat of more than 450 m during the study period. These results provide evidence of the glacier's rapid thinning, reflecting the broader trend of accelerated glacial retreat driven by climate change in the European Alps. This research enriches our understanding of the dynamics and mechanisms of alpine glacial degradation in response to rising global temperatures by providing a detailed, multi-temporal perspective on the glacier's evolution. Beyond its scientific contributions to glaciology, this study highlights the practical potential of UAV-based photogrammetric monitoring as a scalable, cost-effective tool to study remote or inaccessible areas, such as landslides, rockfalls and volcanoes. Future research could build on these findings by integrating additional data sources, such as satellite imagery to complement UAV surveys and improve spatial–temporal coverage. Furthermore, applying these methods to other glaciers in different climatic and topographical contexts could provide a broader comparative framework to investigate regional and global patterns of glacial changes.

CRediT authorship contribution statement

Valeria Belloni: Writing – original draft, Validation, Software, Methodology, Investigation, Formal analysis, Data curation, Conceptualization, Writing – review & editing. **Davide Fugazza:** Writing – original draft, Validation, Software, Methodology, Investigation, Formal analysis, Data curation, Conceptualization, Writing – review & editing. **Kevin Hanson:** Software, Data curation. **Marco Scaioni:** Data curation, Supervision, Writing – review & editing. **Martina Di Rita:** Software, Data curation, Conceptualization, Supervision, Writing – review & editing.

Declaration of competing interest

The authors declare that they have no known competing financial interests or personal relationships that could have appeared to influence the work reported in this paper.

Acknowledgements

The present study was partially supported by Levissima Sanpellegrino S.P.A. through an agreement with the University of Milan. We thank Leica Geosystems AG for for supporting the 2020, 2021, 2022 data collection campaigns by providing GS18 GNSS sensors, Infinity

software and use of HxGN SmartNet GNSS data services. We acnowledge Stelvio Park Authority for permitting the surveys and for support through the project Parco Dello Stelvio - Laboratorio a Cielo Aperto. The authors acknowledge support from the University of Milan through the APC initiative.

Data availability

The authors do not have permission to share data.

References

Agisoft, 2024. Agisoft Metashape user manual - Professional edition, Version 2.1. Technical Report, Agisoft.

Aguilar, F.J., Aguilar, M.A., Fernandez, I., Negreiros, J.G., Delgado, J., Pérez, J.L., 2012. A new two-step robust surface matching approach for three-dimensional georeferencing of historical digital elevation models. IEEE Geosci. Remote. Sens. Lett. 9 (4), 589–593. http://dx.doi.org/10.1109/LGRS.2011.2175899.

Akca, D., 2010. Co-registration of surfaces by 3D least squares matching. Photogramm. Eng. Remote Sens. 76, 307–318. http://dx.doi.org/10.14358/PERS.76.3.307.

Andaru, R., Rau, J.-Y., Chuang, L.Z.-H., Jen, C.-H., 2022. Multitemporal UAV photogrammetry for sandbank morphological change analysis: Evaluations of camera calibration methods, co-registration strategies, and the reconstructed DSMs. IEEE J. Sel. Top. Appl. Earth Obs. Remote. Sens. 15, 5924–5942. http://dx.doi.org/10.1109/JSTARS.2022.3192264.

ASP, 2025. 16.54. pc_align — Ames stereo pipeline "3.5.0-alpha" documentation. URL https://stereopipeline.readthedocs.io/en/latest/tools/pc{_}align.html.

Azzoni, R.S., Fugazza, D., Zennaro, M., Zucali, M., D'Agata, C., Maragno, D., Cernuschi, M., Smiraglia, C., Diolaiuti, G.A., 2017. Recent structural evolution of Forni Glacier tongue (Ortles-Cevedale Group, Central Italian Alps). J. Maps 13 (2), 870–878. http://dx.doi.org/10.1080/17445647.2017.1394227.

Bash, E.A., Moorman, B.J., Gunther, A., 2018. Detecting short-term surface melt on an arctic glacier using UAV surveys. Remote. Sens. 10 (10), http://dx.doi.org/10.3390/rs10101547.

Bearzot, F., Garzonio, R., Di Mauro, B., Colombo, R., Cremonese, E., Crosta, G.B., Delaloye, R., Hauck, C., Morra Di Cella, U., Pogliotti, P., Frattini, P., Rossini, M., 2022. Kinematics of an Alpine rock glacier from multi-temporal UAV surveys and GNSS data. Geomorphology 402, 108116. http://dx.doi.org/10.1016/j.geomorph.2022.108116.

Belloni, V., Di Rita, M., Fugazza, D., Traversa, G., Hanson, K., Diolaiuti, G., Crespi, M., 2023. High-resolution high-accuracy orthophoto map and digital surface model of Forni Glacier tongue (Central Italian Alps) from UAV photogrammetry. J. Maps 19 (1), 2217508. http://dx.doi.org/10.1080/17445647.2023.2217508.

Belloni, V., Fugazza, D., Di Rita, M., 2022. UAV-based glacier monitoring: GNSS kinematic track post-processing and direct georeferencing for accurate reconstructions in challenging environments. Int. Arch. Photogramm. Remote. Sens. Spat. Inf. Sci. XLIII-B1-2022, 367–373. http://dx.doi.org/10.5194/isprs-archives-XLIII-B1-2022-367-2022.

Benoit, L., Gourdon, A., Vallat, R., Irarrazaval, I., Gravey, M., Lehmann, B., Prasicek, G., Gräff, D., Herman, F., Mariethoz, G., 2019. A high-resolution image time series of the Gorner Glacier - Swiss Alps - derived from repeated unmanned aerial vehicle surveys. Earth Syst. Sci. Data 11, 579–588. http://dx.doi.org/10.5194/essd-11-579-2019.

Berthier, E., Arnaud, Y., Kumar, R., Ahmad, S., Wagnon, P., Chevallier, P., 2007. Remote sensing estimates of glacier mass balances in the Himachal Pradesh (Western Himalaya, India). Remote Sens. Environ. 108 (3), 327–338. http://dx.doi.org/10.1016/j.rse.2006.11.017.

Besl, P., McKay, N.D., 1992. A method for registration of 3-D shapes. IEEE Trans. Pattern Anal. Mach. Intell. 14 (2), 239–256. http://dx.doi.org/10.1109/34.121791.

Beyer, R.A., Alexandrov, O., McMichael, S., 2018. The Ames Stereo Pipeline: NASA's open source software for deriving and processing terrain data. Earth Space Sci. 5 (9), 537–548. http://dx.doi.org/10.1029/2018EA000409.

Bondesan, A., Francese, R.G., 2023. The climate-driven disaster of the Marmolada Glacier (Italy). Geomorphology 431, 108687. http://dx.doi.org/10.1016/j.geomorph.2023.108687.

Brun, F., Wagnon, P., Berthier, E., Shea, J.M., Immerzeel, W.W., Kraaijenbrink, P.D.A., Vincent, C., Reverchon, C., Shrestha, D., Arnaud, Y., 2018. Ice cliff contribution to the tongue-wide ablation of Changri Nup Glacier, Nepal, central Himalaya. Cryosphere 12 (11), 3439–3457. http://dx.doi.org/10.5194/tc-12-3439-2018.

Che, Y., Wang, S., Yi, S., Wei, Y., Cai, Y., 2020. Summer mass balance and surface velocity derived by unmanned aerial vehicle on debris-covered region of Baishui River Glacier No. 1, Yulong Snow Mountain. Remote. Sens. 12 (20), 3280–3294. http://dx.doi.org/10.3390/rs12203280.

Crosta, A., De Felice, B., Antonioli, D., Chiarcos, R., Perin, E., Ortenzi, M.A., Gazzotti, S., Azzoni, R.S., Fugazza, D., Gianotti, V., Laus, M., Diolaiuti, G., Pittino, F., Franzetti, A., Ambrosini, R., Parolini, M., 2022. Microplastic contamination of supraglacial debris differs among glaciers with different anthropic pressures. Sci. Total Environ. 851, 158301. http://dx.doi.org/10.1016/j.scitotenv.2022.158301.

D'Agata, C., Bocchiola, D., Soncini, A., Maragno, D., Smiraglia, C., Diolaiuti, G.A., 2018. Recent area and volume loss of Alpine glaciers in the Adda River of Italy and their contribution to hydropower production. Cold Reg. Sci. & Technol. 148, 172–184. http://dx.doi.org/10.1016/j.coldregions.2017.12.010.

Dall'Asta, E., Forlani, G., Roncella, R., Santise, M., Diotri, F., Morra di Cella, U., 2017. Unmanned Aerial Systems and DSM matching for rock glacier monitoring. ISPRS J. Photogramm. Remote Sens. 127, 102–114. http://dx.doi.org/10.1016/j.isprsjprs.2016.10.003.

De Gaetani, C.I., Ioli, F., Pinto, L., 2021. Aerial and UAV images for photogrammetric analysis of Belvedere Glacier evolution in the period 1977–2019. Remote. Sens. 13 (18), http://dx.doi.org/10.3390/rs13183787.

Di Mauro, B., Fugazza, D., 2022. Pan-Alpine glacier phenology reveals lowering albedo and increase in ablation season length. Remote Sens. Environ. 279, 113119. http://dx.doi.org/10.1016/j.rse.2022.113119.

Di Rita, M., Fugazza, D., Belloni, V., Diolaiuti, G., Scaioni, M., Crespi, M., 2020. Glacier volume change monitoring from UAV observations: issues and potentials of state-of-the-art techniques. Int. Arch. Photogramm. Remote. Sens. Spat. Inf. Sci. XLIII-B2-2020, 1041–1048. http://dx.doi.org/10.5194/isprs-archives-XLIII-B2-2020-1041-2020.

Diolaiuti, G., Smiraglia, C., 2010. Changing glaciers in a changing climate: how vanishing geomorphosites have been driving deep changes in mountain landscapes and environments. Géomorphologie : Relief, Process. Environ. 16 (2), 131–152. http://dx.doi.org/10.4000/geomorphologie.7882.

Egli, P.E., Belotti, B., Ouvry, B., Irving, J., Lane, S.N., 2021. Subglacial channels, climate warming, and increasing frequency of alpine glacier snout collapse. Geophys. Res. Lett. 48 (21), http://dx.doi.org/10.1029/2021GL096031.

Eskandari, R., Genzano, N., Fugazza, D., Scaioni, M., 2024. Investigation on Miage/Brenva Glaciers in the Alps from 50s to-date based on remote-sensing data. In: Int. Arch. Photogramm. Remote Sens. Spatial Inf. Sci., Vol. XLVIII, Part 3-2024. pp. 147–154. http://dx.doi.org/10.5194/isprs-archives-XLVIII-3-2024-147-2024.

Feurer, D., Vinatier, F., 2018. Joining multi-epoch archival aerial images in a single SfM block allows 3-D change detection with almost exclusively image information. ISPRS J. Photogramm. Remote Sens. 146, 495–506. http://dx.doi.org/10.1016/j.isprsjprs.2018.10.016.

Fey, C., Krainer, K., 2020. Analyses of UAV and GNSS based flow velocity variations of the rock glacier Lazaun (Ötztal Alps, South Tyrol, Italy). Geomorphology 365, 107261. http://dx.doi.org/10.1016/j.geomorph.2020.107261.

Franzetti, A., Navarra, F., Tagliaferri, I., Gandolfi, I., Bestetti, G., Minora, U., Azzoni, R.S., Diolaiuti, G., Smiraglia, C., Ambrosini, R., 2017. Potential sources of bacteria colonizing the cryoconite of an Alpine glacier. PLOS ONE 12 (3), e0174786. http://dx.doi.org/10.1371/journal.pone.0174786.

Fu, Y., Liu, Q., Liu, G., Zhang, B., Zhang, R., Cai, J., Wang, X., Xiang, W., 2022. Seasonal ice dynamics in the lower ablation zone of Dagongba Glacier, southeastern Tibetan Plateau, from multitemporal UAV images. J. Glaciol. 68 (270), 636–650. http://dx.doi.org/10.1017/jog.2021.123.

Fugazza, D., Scaioni, M., Corti, M., D'Agata, C., Azzoni, R.S., Cernuschi, M., Smiraglia, C., Diolaiuti, G.A., 2018. Combination of UAV and terrestrial photogrammetry to assess rapid glacier evolution and map glacier hazards. Nat. Hazards Earth Syst. Sci. 18 (4), 1055–1071. http://dx.doi.org/10.5194/nhess-18-1055-2018.

Fugazza, D., Troilo, F., 2024. Extreme thinning of the Brenva Glacier tongue from repeat UAV DEMs. In: Trends in Earth Observation. vol. 3, AIT, pp. 38–41.

Geissler, J., Mayer, C., Jubanski, J., Münzer, U., Siegert, F., 2021. Analyzing glacier retreat and mass balances using aerial and UAV photogrammetry in the Ötztal Alps, Austria. Cryosphere 15 (8), 3699–3717. http://dx.doi.org/10.5194/tc-15-3699-2021.

Genzano, N., Fugazza, D., Eskandari, R., Scaioni, M., 2024. Multitemporal Structure-from-Motion: A flexible tool to cope with aerial blocks in changing mountain environment. Int. Arch. Photogramm. Remote. Sens. Spat. Inf. Sci. XLVIII-2-2024, 99–106. http://dx.doi.org/10.5194/isprs-archives-XLVIII-2-2024-99-2024.

Gobbi, M., Lencioni, V., 2021. Glacial biodiversity: Lessons from ground-dwelling and aquatic insects. In: Kanao, M., Godone, D., Dematteis, N. (Eds.), Glaciers and the Polar Environment. IntechOpen, pp. 143–165. http://dx.doi.org/10.5772/intechopen.92826.

Gruen, A., Akca, D., 2005. Least squares 3D surface and curve matching. ISPRS J. Photogramm. Remote Sens. 59 (3), 151–174. http://dx.doi.org/10.1016/j.isprsjprs.2005.02.006.

Immerzeel, W., Kraaijenbrink, P., Shea, J., Shrestha, A., Pellicciotti, F., Bierkens, M., de Jong, S., 2014. High-resolution monitoring of Himalayan glacier dynamics using unmanned aerial vehicles. Remote Sens. Environ. 150, 93–103. http://dx.doi.org/10.1016/j.rse.2014.04.025.

Ioli, F., Bianchi, A., Cina, A., De Michele, C., Maschio, P., Passoni, D., Pinto, L., 2022. Mid-term monitoring of glacier's variations with UAVs: The example of the Belvedere Glacier. Remote. Sens. 14 (1), http://dx.doi.org/10.3390/rs14010028.

James, M., Robson, S., 2012. Straightforward reconstruction of 3D surfaces and topography with a camera: Accuracy and geoscience application. J. Geophys. Res. 117, F03017. http://dx.doi.org/10.1029/2011JF002289.

Karimi, N., Sheshangosht, S., Roozbahani, R., 2021. High-resolution monitoring of debris-covered glacier mass budget and flow velocity using repeated UAV photogrammetry in Iran. Geomorphology 389, 107855. http://dx.doi.org/10.1016/j.geomorph.2021.107855.

Karkee, M., Steward, B.L., Aziz, S.A., 2008. Improving quality of public domain digital elevation models through data fusion. Biosyst. Eng. 101 (3), 293–305. http://dx.doi.org/10.1016/j.biosystemseng.2008.09.010.

Kraaijenbrink, P., Meijer, S.W., Shea, J.M., Pellicciotti, F., De Jong, S.M., Immerzeel, W.W., 2016. Seasonal surface velocities of a Himalayan glacier derived by automated correlation of unmanned aerial vehicle imagery. Ann. Glaciol. 57 (71), 103–113. http://dx.doi.org/10.3189/2016AoG71A072.

Lamsters, K., Ješkins, J., Sobota, I., Karušs, J., Džeriņ˘ s, P., 2022. Surface characteristics, elevation change, and velocity of high-arctic valley glacier from repeated high-resolution UAV photogrammetry. Remote. Sens. 14 (4), http://dx.doi.org/10.3390/rs14041029.

Li, H., Deng, Q., Wang, L., 2017. Automatic co-registration of digital elevation models based on centroids of subwatersheds. IEEE Trans. Geosci. Remote Sens. 55 (11), 6639–6650. http://dx.doi.org/10.1109/TGRS.2017.2731048.

Li, T., Hu, Y., Liu, B., Jiang, L., Wang, H., Shen, X., 2023. Co-registration and residual correction of digital elevation models: a comparative study. Cryosphere 17 (12), 5299–5316. http://dx.doi.org/10.5194/tc-17-5299-2023.

Micheletti, N., Chandler, J., Lane, S.N., 2015. Structure from motion (SFM) photogrammetry. In: E., C.L., J.M., N. (Eds.), Geomorphological Techniques. British society for geomorphology, London, pp. 1–12.

Milner, A.M., Khamis, K., Battin, T.J., Brittain, J.E., Barrand, N.E., Füreder, L., Cauvy-Fraunié, S., Gíslason, G.M., Jacobsen, D., Hannah, D.M., Hodson, A.J., Hood, E., Lencioni, V., Ólafsson, J.S., Robinson, C.T., Tranter, M., Brown, L.E., 2017. Glacier shrinkage driving global changes in downstream systems. Proc. Natl. Acad. Sci. 114 (37), 9770–9778. http://dx.doi.org/10.1073/pnas.1619807114.

Nuth, C., Kääb, A., 2011. Co-registration and bias corrections of satellite elevation data sets for quantifying glacier thickness change. Cryosphere 5 (1), 271–290. http://dx.doi.org/10.5194/tc-5-271-2011.

Paul, F., Rastner, P., Azzoni, R.S., Diolaiuti, G., Fugazza, D., Le Bris, R., Nemec, J., Rabatel, A., Ramusovic, M., Schwaizer, G., Smiraglia, C., 2020. Glacier shrinkage in the Alps continues unabated as revealed by a new glacier inventory from Sentinel-2. Earth Syst. Sci. Data 12 (3), 1805–1821. http://dx.doi.org/10.5194/essd-12-1805-2020.

Pomerleau, F., Colas, F., Siegwart, R., Magnenat, S., 2013. Comparing ICP variants on realworld data sets. Auton. Robots 34, 133–148. http://dx.doi.org/10.1007/s10514-013-9327-2.

Rossini, M., Di Mauro, B., Garzonio, R., Baccolo, G., Cavallini, G., Mattavelli, M., De Amicis, M., Colombo, R., 2018. Rapid melting dynamics of an Alpine glacier with repeated UAV photogrammetry. Geomorphology 304, 159–172. http://dx.doi.org/10.1016/j.geomorph.2017.12.039.

Salim, E., 2023. Glacier tourism without ice: Envisioning future adaptations in a melting world. Front. Hum. Dyn. 5, http://dx.doi.org/10.3389/fhumd.2023.1137551.

Scaioni, M., Barazzetti, L., Yordanov, V., Azzoni, R.S., Fugazza, D., Cernuschi, M., Diolaiuti, G.A., 2019. Structure-from-Motion photogrammetry to support the assessment of collapse risk in Alpine glaciers. In: Altan, O., Chandra, M., Sunar, F., Tanzi, T.J. (Eds.), Intelligent Systems for Crisis Management. Springer International Publishing, Cham, pp. 239–263. http://dx.doi.org/10.1007/978-3-030-05330-7_10.

Scaioni, M., Corti, M., Diolaiuti, G., Fugazza, D., Cernuschi, M., 2017. Local and general monitoring of Forni Glacier (Italian alps) using multi-platform Structure-from-Motion photogrammetry. Int. Arch. Photogramm. Remote. Sens. Spat. Inf. Sci. XLII-2/W7, 1547–1554. http://dx.doi.org/10.5194/isprs-archives-XLII-2-W7-1547-2017.

Schaefli, B., Manso, P., Fischer, M., Huss, M., Farinotti, D., 2019. The role of glacier retreat for Swiss hydropower production. Renew. Energy 132, 615–627. http://dx.doi.org/10.1016/j.renene.2018.07.104.

Securo, A., Del Gobbo, C., Rettig, L., Pillon, S., De Luca, A., Fontana, D., Benedetti Fasil, E., Colucci, R.R., 2024. A glacier in transition: Surface elevation change, ELA and geomorphic evolution of a very small glacier in the Dolomites (S-E Alps). Geomorphology 444, 108956. http://dx.doi.org/10.1016/j.geomorph.2023.108956.

Senese, A., Pelfini, M., Maragno, D., Bollati, I.M., Fugazza, D., Vaghi, L., Federici, M., Grimaldi, L., Belotti, P., Lauri, P., Ferliga, C., La Rocca, L., Diolaiuti, G.A., 2023. The role of E-bike in discovering geodiversity and geoheritage. Sustainability 15 (6), 4979. http://dx.doi.org/10.3390/su15064979.

Shean, D.E., Alexandrov, O., Moratto, Z.M., Smith, B.E., Joughin, I.R., Porter, C., Morin, P., 2016. An automated, open-source pipeline for mass production of digital elevation models (DEMs) from very-high-resolution commercial stereo satellite imagery. ISPRS J. Photogramm. Remote Sens. 116, 101–117. http://dx.doi.org/10.1016/j.isprsjprs.2016.03.012.

Shean, D.E., Bhushan, S., Montesano, P., Rounce, D.R., Arendt, A., Osmanoglu, B., 2020. A systematic, regional assessment of high mountain Asia glacier mass balance. Front. Earth Sci. 7, http://dx.doi.org/10.3389/feart.2019.00363.

Shean, D.E., Joughin, I.R., Dutrieux, P., Smith, B.E., Berthier, E., 2019. Ice shelf basal melt rates from a high-resolution digital elevation model (DEM) record for Pine Island Glacier, Antarctica. Cryosphere 13 (10), 2633–2656. http://dx.doi.org/10.5194/tc-13-2633-2019.

Van Tricht, L., Huybrechts, P., Van Breedam, J., Vanhulle, A., Van Oost, K., Zekollari, H., 2021. Estimating surface mass balance patterns from unoccupied aerial vehicle measurements in the ablation area of the Morteratsch-Pers Glacier complex (Switzerland). Cryosphere 15 (9), 4445–4464. http://dx.doi.org/10.5194/tc-15-4445-2021.

Vincent, C., Wagnon, P., Shea, J.M., Immerzeel, W.W., Kraaijenbrink, P., Shrestha, D., Soruco, A., Arnaud, Y., Brun, F., Berthier, E., Sherpa, S.F., 2016. Reduced melt on debris-covered glaciers: investigations from Changri Nup Glacier, Nepal. Cryosphere 10 (4), 1845–1858. http://dx.doi.org/10.5194/tc-10-1845-2016.

Vivero, S., Lambiel, C., 2024. Annual surface elevation changes of rock glaciers and their geomorphological significance: Examples from the Swiss Alps. Geomorphology 467, 109487. http://dx.doi.org/10.1016/j.geomorph.2024.109487.

Westoby, M.J., Brasington, J., Glasser, N.F., Hambrey, M.J., Reynolds, J.M., 2012. Structure-from-Motion photogrammetry: A low-cost, effective tool for geoscience applications. Geomorphology 179, 300–314. http://dx.doi.org/10.1016/j.geomorph.2012.08.021.

Westoby, M.J., Rounce, D.R., Shaw, T.E., Fyffe, C.L., Moore, P.L., Stewart, R.L., Brock, B.W., 2020. Geomorphological evolution of a debris-covered glacier surface. Earth Surf. Process. Landf. 45 (14), 3431–3448. http://dx.doi.org/10.1002/esp.4973.

Wu, B., Guo, J., Hu, H., Li, Z., Chen, Y., 2013. Co-registration of lunar topographic models derived from Chang'E-1, SELENE, and LRO laser altimeter data based on a novel surface matchingmethod. Earth Planet. Sci. Lett. 364, 68–84. http://dx.doi.org/10.1016/j.epsl.2012.12.024.